Mapping Molecular Differences and Extracellular Matrix Gene Expression in Segmental Outflow Pathways of the Human Ocular Trabecular Meshwork

Janice A. Vranka*, John M. Bradley, Yong-Feng Yang, Kate E. Keller, Ted S. Acott

Casey Eye Institute, Oregon Health & Science University, 3181 SW Sam Jackson Park Rd, Portland, Oregon, United States of America

* vranka@ohsu.edu

Abstract

Elevated intraocular pressure (IOP) is the primary risk factor for glaucoma, and lowering IOP remains the only effective treatment for glaucoma. The trabecular meshwork (TM) in the anterior chamber of the eye regulates IOP by generating resistance to aqueous humor outflow. Aqueous humor outflow is segmental, but molecular differences between high and low outflow regions of the TM are poorly understood. In this study, flow regions of the TM were characterized using fluorescent tracers and PCR arrays. Anterior segments from human donor eyes were perfused at physiological pressure in an *ex vivo* organ culture system. Fluorescently-labeled microspheres of various sizes were perfused into anterior segments to label flow regions. Actively perfused microspheres were segmentally distributed, whereas microspheres soaked passively into anterior segments uniformly labeled the TM and surrounding tissues with no apparent segmentation. Cell-tracker quantum dots (20 nm) were localized to the outer uveal and corneoscleral TM, whereas larger, modified microspheres (200 nm) localized throughout the TM layers and Schlemm's canal. Distribution of fluorescent tracers demonstrated a variable labeling pattern on both a macro- and micro-scale. Quantitative PCR arrays allowed identification of a variety of extracellular matrix genes differentially expressed in high and low flow regions of the TM. Several collagen genes (COL16A1, COL4A2, COL6A1 and 2) and MMPs (1, 2, 3) were enriched in high, whereas COL15A1, and MMP16 were enriched in low flow regions. Matrix metalloproteinase activity was similar in high and low regions using a quantitative FRET peptide assay, whereas protein levels in tissues showed modest regional differences. These gene and protein differences across regions of the TM provide further evidence for a molecular basis of segmental flow routes within the aqueous outflow pathway. New insight into the molecular mechanisms of segmental aqueous outflow may aid in the design and delivery of improved treatments for glaucoma patients.

and analysis, decision to publish, or preparation of the manuscript.

Introduction

In the human eye, the majority of aqueous humor fluid (approximately 90%) exits the anterior chamber via the conventional outflow pathway, which drains aqueous fluid through the filter-like trabecular meshwork (TM) tissue to Schlemm's canal.[1] The TM can be divided into 3 separate regions based on location and structure: 1) the outer uveal meshwork, and 2) the deeper corneoscleral meshwork, both regions containing fenestrated beams of lamellae and large, open intertrabecular spaces, and 3) the juxtacanalicular tissue (JCT) that is directly adjacent to the inner wall endothelium of Schlemm's canal. [2–4] It is composed of JCT cells embedded in a loosely arranged extracellular matrix. Intraocular pressure (IOP) is generated by building resistance to aqueous humor outflow in the TM.[2,5] Aqueous humor outflow resistance is believed to reside within the 7–14 μm of the inner wall of Schlemm's canal, which is the approximate thickness of the JCT.[2,5–8] The extracellular matrix (ECM) of the JCT is thought to be integrally and extensively involved in generating the outflow resistance, since disrupting it by several methods has been shown to affect outflow resistance.[2,9–11] For example, perfusion of MMPs or their inhibitors resulted in increased or decreased outflow, respectively[9], whereas over-expression of MMP in a steroid-inducible adenovirus increased outflow in perfused anterior segments.[12] In anterior segment organ culture, outflow facility (C) is defined as the flow rate divided by the perfusion pressure, and is inversely proportional to outflow resistance. Glycosaminoglycans (GAGs) and proteoglycans were implicated as integral molecular components of the resistance by perfusion of GAG-degrading enzymes, which increased outflow facility in animals [13–15] Studies using RNAi gene silencing and chemical inhibitors to modify the GAG biosynthesis and structure elicited similar responses on outflow in humans.[3,11,16]

Versican is a large chondroitin sulfate proteoglycan and a component of the ECM of the TM.[17,18] Perfusion of versican RNAi silencing lentivirus or a recombinant HepII domain of fibronectin into human anterior segment organ culture, has been shown to have a direct effect on outflow implicating versican and fibronectin as components of the resistance.[17,19] Additionally, matrix metalloproteinases (MMPs) perfused into anterior segment organ culture increased outflow facility, whereas perfusion of inhibitors of MMPs reduced outflow facility.[9] MMPs -1, -3, -9, and ADAMTS4 have also been shown to be up-regulated, activated, and released in response to increased pressure.[3,10,20] Increase and activation of these enzymes likely target structural ECM proteins of the TM. For example, MMPs -2 and -14 degrade collagen and ADAMTS4 degrades versican, to allow greater aqueous humor outflow. Thus, multiple molecular components of the abundant ECM within the TM are the likely source of aqueous outflow resistance.

Aqueous humor outflow has long been known to be segmental in nature with regions of relatively high and relatively low aqueous outflow around the circumference of the outflow pathway.[21–25] Non-uniform patterns of aqueous humor outflow appear to be universal as they have been demonstrated in mouse, porcine, bovine, monkey and human eyes.[17,26–31] Pigmentation of trabecular meshwork cells was suggested to be a marker for preferential aqueous flow pathways; however, such pigmented regions were not shown to differ in trabecular cell number or ultrastructural characteristics when compared with non-pigmented regions of the aqueous outflow pathway in the same individual.[23,32] Multiple tracers have been used to study the variation in flow including zymosan, latex microspheres, cationic ferritin and fluorescent Qdots. However, cationic ferritin has been used most frequently because of its small size (12nm) and its ability to bind to negatively charged membrane surfaces.[22,24,33–36] In one of the earliest studies done in human eyes, perfusion of cationic ferritin showed the aqueous outflow pathway from glaucomatous eyes to have more segmental variation in the labeling as compared with the outflow pathway from normal human eyes; however, no obvious morphologic

changes were associated with the regional changes in cationic ferritin labeling.[34] In support of these findings, another study examined the regional morphological differences in the aqueous outflow pathway and TM around the circumference of the eye and found no significant segmental differences within the aqueous outflow pathway of either normal or glaucomatous individuals in terms of overall ultrastructural distributions.[21] Cationic ferritin perfusion was shown to reduce outflow facility in contrast to perfusion of anionic ferritin, which had no effect on facility, although both showed highly variable distributions around the eye.[22] More recently, studies using dextran beads or fluorescent microspheres perfused into bovine eyes have demonstrated segmental distribution of microspheres at pressures of 15 mmHg and above, [26,27,30,31] and in human eyes at 7 and 30 mmHg.[37] Finally, perfusion of viruses and the pattern of expression of reporter proteins also appear to be segmental.[17,38,39]

In spite of these observations, little is known about how the segmental pattern arises. We hypothesized that the molecular composition in areas of high or low outflow must be different, which either affects or reflects the pattern of outflow. Expression of the proteoglycan versican, was shown to be inversely correlated with outflow regions in human anterior segment organ culture.[17] Additionally, secreted protein acidic and rich in cysteine (SPARC) null mice have recently been shown to have more uniform outflow compared to wild-type littermates suggesting that SPARC may also display segmental differences in expression.[29] Moreover, fibronectin and hyaluronan binding protein were found to have variable patterns of immunostaining, although this was not correlated with tracers.[11,40] The purpose of this study was to further define the nature of segmental fluid flow in the human outflow pathway and correlate patterns of ECM gene expression and proteolytic enzyme activity with high and low flow regions of the TM.

Materials and Methods

Anterior segment perfusion culture

Anterior segment perfusion culture is an established technique to study outflow facility *ex vivo*. [10,11,16,17,41] Use of human donor eye tissue was approved by Oregon Health & Science University Institutional Review Board and experiments were conducted in accordance with the tenets of the Declaration of Helsinki for the use of human tissue. Human eye tissue was obtained from cadavers (Lions VisionGift, Portland, OR). Length of time from death to stationary culture was limited 48 hours or less. Anterior segments were placed into serum-free stationary organ culture for 5–7 days to facilitate recovery post-mortem. The age range was 65–97 years and average age of the cadaver eyes for all experiments in this study was 76.29 ± 8.7 years (n = 14). All relevant biological information regarding the donor and known ocular history is listed (S1 Table). Exclusion criteria for donor eyes was: 1) glaucomatous and glaucoma-suspect eyes were not included, and 2) perfused eyes whose flow rates were outside of the range of 1–9 μl/min (or whose facility was outside of the range of 0.125–1.0 μl/min/mm Hg) were excluded from this study. Human anterior segments were perfused with serum-free Dulbecco's Modified Eagle's Medium (DMEM) containing 1% Penicillin/Streptomycin/Fungizone, at constant pressure (8.8 mmHg) with an average flow rate of 1–7 μl/min, which is similar to normal physiological rate and pressures (minus episcleral venous pressure) *in vivo*.[11] Data from individual eyes were combined where possible and representative images were used. The number of eyes used for each treatment is noted in the figure legend.

Tracer Labeling

Anterior segments were perfused continuously, unless otherwise noted, for approximately 5 days. During the final stage of perfusion, fluorescently-labeled microspheres (Invitrogen, Carlsbad, CA) were diluted 1:1000 into PBS, vortexed vigorously, and 200μl of that mixture was

injected as a bolus directly in-line into the anterior segment organ culture and perfused for 1 hour. In the case of the soak labeling, the anterior segments were removed from perfusion and allowed to soaking overnight at 37ºC in the fluorescent tracer diluted 1:1000 in PBS. The following day, perfusion was resumed. In the case of the sequential labeling, the first label was perfused in for 1 hour, and then the line and reservoir were washed twice with PBS. The second fluorescent label was then perfused in for 1 hour. The time between sequential labelings was approximately 60 minutes. The labels used in this study are in Table 1.

Immunofluorescence and Microscopy

At the end of perfusion, TM tissue intended for immunohistochemistry and confocal imaging, was immersion-fixed in 4% paraformaldehyde/PBS for 1 hour at 25ºC. Fluorescent labeling of whole anterior segments were imaged *en face* using a Leica DM500 microscope prior to cutting into 10–12 radial wedges. Frontal sections were then cut with a single-edged razor blade perpendicular to the ocular surface, resulting in a section tangential to the corneoscleral limbus that bisects Schlemm's canal as described previously.[16,17,27,29] After labeling anterior segments with fluorescent microspheres in organ culture, followed by fixation (as described above), immunostaining was performed as follows. Tissues were incubated in CAS-Block, a universal blocking reagent to saturate the non-specific binding sites (Invitrogen, Grand Island, NY), for 1 hour at room temperature, and then incubated overnight at 4ºC with one or more of the following antibodies: a versican mouse monoclonal antibody (12C5), a platelet endothelial cell adhesion molecule (PECAM) mouse monoclonal antibody (P2B1), a type VI collagen mouse monoclonal antibody (5C6), and an osteopontin (SPP1) mouse monoclonal antibody (MPIIIB10) all purchased from Developmental Studies Hybridoma Bank, Iowa City, IA, a fibrillin1 mouse monoclonal antibody (MAB1919) purchased from Millipore (Temecula, CA), a SPARC rabbit polyclonal antibody (15274-1-AP) purchased from Proteintech Group (Chicago, IL) or a MMP3 rabbit polyclonal antibody (AAS41420C) from purchased from Antibody Verify (Las Vegas, NV). The PECAM antibody was used as a biomarker of Schlemm's canal. [42] Primary antibodies were detected with Alexa-fluor 488-conjugated anti-mouse or anti-rabbit secondary antibodies (Invitrogen, Grand Island, NY). Tissue wedges were placed on 0.17 mm Delta T cover glass bottom culture dishes from Bioptechs Inc. (Butler, PA) in Slow-fade Gold antifade reagent with DAPI (Invitrogen), and imaged by confocal microscopy using an Olympus FV1000 microscope. Optical sections were acquired using sequential scanning in separate laser channels. Image acquisition settings and number of optical sections in a stack were kept constant when comparing images. Micro-scale analysis of high flow regions was performed by selecting images of high flow regions using Image J software and "Plot Profile" to

Table 1. Fluorescent microspheres of varying size and modification used in this study.

Label	Color (Ex/Em)	Modification	Size (nm)
Q-Tracker-655	Red (405-615/655)	HIV-Tat	20
Q-Tracker-585	Green (405-545/585)	HIV-Tat	20
Q-Tracker-525	Yellow-Green (505/515)	HIV-Tat	20
Q-dot-655	Red (405-615/655)	ITK amino	20
Fluospheres	Yellow-Green (505/515)	Amine	200
Fluospheres	Red (580/605)	Amine	200
Fluospheres	Red (580/605)	Carboxylate	500
Fluospheres	Yellow-Green (505/515)	Carboxylate	20
Fluospheres	Yellow-Green (505/515)	Carboxylate	200

doi:10.1371/journal.pone.0122483.t001

get graphical output of distance (in μm) versus relative fluorescence intensity. Additionally, confocal images were analyzed using Imaris Bitplane 3-D software (South Windsor, CT) to generate Pearson's correlation coefficients with selected color channels, as has been described previously.[43] The Pearson's correlation coefficient is a quantitative statistic relating the degree of overlap between fluorescence signals from two different color channels.[44] Pearson's coefficient values range from 1.0, indicating complete colocalization, 0, indicating no significant correlation, to -1, indicating complete separation of two signals.[44,45] A Pearson's correlation coefficient was calculated for each fluorescently-labeled tracer paired with versican immunostaining from raw compressed confocal z-stacks. The Pearson coefficients were averaged and a standard error of the mean was calculated (n = 4).

Quantitative PCR Arrays

Human anterior segments were mounted for perfusion culture and perfused at constant pressure (8 mmHg) for 48 hours. Amine-modified 200 nm fluorescent microspheres (Invitrogen; 1:1000 dilution) were injected into the perfusion line and perfused into the anterior segments for 60 minutes. Flow was then stopped, and eyes were removed from the organ culture system and viewed *en face* under a fluorescent microscope (Leica DM500, Wetzlar, Germany). Wedges of tissue were cut with a razor blade to separate low and high flow regions of TM. The TM was then dissected from the tissue wedge and RNA was extracted using TRIzol (Life Technologies, Grand Island, NY) according to the manufacturer's instructions. Total RNA was quantified using a Nanodrop 2000 Spectrophotometer (Thermoscientific, Waltham, MA). Approximately 100 ng total RNA was used as a template for amplification using MessageAmp II aRNA Amplification Kit (Ambion Inc., Life Technologies, Grand Island, NY) according to the manufacturer's instructions. Equal amounts of amplified RNA (from high and low flow regions of the trabecular meshwork) were reverse transcribed using the RT^2 First Strand Kit (Qiagen, Hilden, Germany), followed by quantitative PCR with a BioRad/MJ Chromo4 PTC-200 Thermocycler using the RT^2 Profiler PCR Array, Human Extracellular Matrix and Adhesion Molecules (Catalog # PAHS-013Z, Qiagen). Each 96-well plate includes 84 pathway focused genes, 5 housekeeping genes, a genomic DNA control, 3 wells containing reverse-transcription controls, and 3 wells containing positive PCR controls. Assays for 5 housekeeping genes included in the arrays enable normalization of the data. The genomic DNA control specifically detects nontranscribed genomic DNA contamination with a high level of sensitivity. The reverse-transcription control is an assay that tests the efficiency of the reverse-transcription reaction performed. PCR data was analyzed using the RT^2 Profiler PCR Array Data Analysis Software, version 3.5 (Qiagen/Sabiosciences), available online at http://www.sabiosciences.com/pcrarraydataanalysis.php. High and low flow regions were selected from 4 different donor eyes and quantitative PCR arrays were performed on each sample. For initial data analysis on the individual PCR arrays, optimal sets of internal control / housekeeping / normalization genes were automatically-selected from each full plate. (The software measures and identifies the genes with the most stable expression via a non-normalized calculation.) The C_t values for these genes are then geometrically averaged and used for the $\Delta\Delta C_t$ calculations, which represent normalized gene expression values for all genes. Fold change values for each experiment were calculated as relative gene levels in high flow regions in comparison with gene levels in low flow regions using the same data analysis software. Fold-changes were averaged and a standard error of the mean was calculated for all genes in the PCR array.

Statistical Analyses

The threshold fold-change differences that were semi-arbitrarily determined to be biologically significant were fold-change values that were greater than 1.5 (i.e., genes enriched in high flow

regions) and less than or equal to 0.5 (i.e., genes enriched in low flow regions.) Initially, all fold-change values were subjected to an unpaired t-test in comparison with a set of genes that had no change across all experiments (fold-change = 1.0). P values <0.05 were determined to be significant. Data were then assessed using Bonferroni to correct for multiple comparisons. Subsequently, we used the more rigorous SAM (significance analysis of microarrays),[46] version 4.01, with 4 biological replicates, to determine statistically significant gene changes for HF and LF regions. We normalized the raw data using the delta delta Ct values for HF and LF regions. The analysis was two class paired, both with arrays median centered and without centering, 500 permutations. 10 nearest neighbors were calculated for K-Nearest Neighbor imputer. Different Delta Values (for adjusting the false discovery rate) were set to be between 0.264 and 0.61 with similar results. SAM was obtained from (http://www-stat.Stanford.EDU/~tibs/SAM). REXCEL 2013, a high-level interface between R and Excel, was obtained from (http://rcom.univie.ac.at/); R is a free software environment for statistical computing and graphics and more can be found at (http://www.r-project.org/). The data obtained with SAM is shown as fold change gene expression, and is in good agreement with the initial fold change values determined as statistically significant by unpaired t-test and Bonferroni.

MMP activity assays

Fluorogenic peptide assays were used to quantitate MMP (Sensolyte 520 generic MMP assay kit, Anaspec, Fremont, CA) activity in low and high flow areas of human tissue perfused with Qtracker 594, as described for human anterior segments above. Human tissue was acquired and anterior segments were perfused in organ culture with fluorescent microspheres. Tissues wedges were separated into areas of high and low flow based on fluorescence intensity and the TMs were dissected. Tissue samples were homogenized in the lysis buffer supplied with the kit. Samples were activated by incubation with APMA (*amino-phenyl mercuric acetate*) for 90 minutes and then incubated with the quenched fluorescence resonance energy transfer (FRET) peptide. The MMP peptide is a substrate for MMPs -1, -2, -3, -7, -8, -9, -10, -12, -13 and -14. Upon MMP cleavage, the peptide generates fluorescence, which was measured using a plate reader (Ex/Em = 490/520 nm). To account for the different sizes of tissue wedge, relative fluorescent units (RFUs) were normalized to total protein concentration (μg/ml) in each sample as measured by the BCA assay (Thermo Fisher Scientific, Rockford, IL). Data from multiple regions (n = 5) were averaged and a standard error of the mean was calculated. Significance was determined using ANOVA, where p < 0.05 was considered significant.

Results

Segmental Flow in Perfused Human Eyes

Segmental flow was visualized circumferentially within the aqueous outflow pathway in a human donor eye after perfusion of the anterior segment in organ culture with Qtracker-655 quantum dots (HIV-TAT labeled) (Fig 1). Examples of regional differences are indicated by brackets. Regions of high and low fluorescence labeling were distinguishable from each other *en face* and correlate with areas of high and low outflow.

We hypothesized that fluorescent microspheres of varying size and different modifications could show differences in their distribution patterns across the various layers of the TM (for example, in the corneoscleral meshwork versus the JCT region), possibly indicating potential flow routes through this tissue. To evaluate this possibility, a variety of fluorescent tracers (Table 1) were perfused into anterior segment organ culture prior to fixation. Frontal sections of tissues were imaged using confocal microscopy to compare their distributions across the various layers of the TM within high and low flow regions (S1 Fig). Qtracker-655 quantum dots
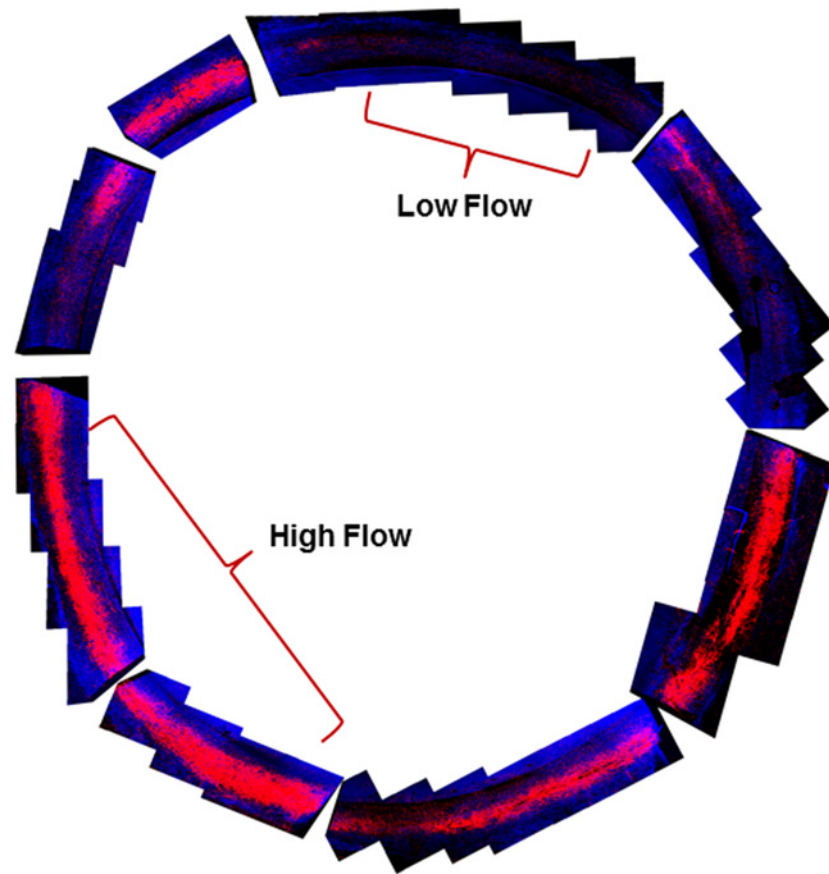
Fig 1. Segmental flow in perfused human eyes. *En face* image of a whole human eye labeled with Qtracker-655 (red) during perfusion. The perfused tissue was cut into approximately 8 wedges and all were imaged *en face* by confocal microscopy. En face images were positionally labeled and then photo-merged digitally to create a collage using Adobe Photoshop software. Regions of high and low labeling demonstrate the segmental nature of outflow with labeled brackets indicating examples of each region. Gaps reflect razor blade cut sites. Blue is autofluorescence of the TM tissue.

(20nm in size) are predominantly localized within the outer uveal TM beams and corneoscleral meshwork in both high and low flow (regions although at dramatically higher levels in high flow regions (S1 Fig). These Qdots are modified with a HIV-TAT peptide to facilitate cellular uptake and they appear to be taken up most effectively by the uveal TM beam cells. In comparison, the 200nm amine-modified fluorescent microspheres localized throughout the various layers of the TM and into Schlemm's canal in high flow regions (S1 Fig). The larger tracers seemed to have a wider distribution throughout the TM, particularly in the high flow regions, whereas the smaller tracers appear to be taken up more aggressively by the outer uveal TM cells. Segmental flow appears to be independent of tracer size and modification, but localization of tracers across the various anatomical layers of the TM is not.

Next, we compared distribution of fluorescent tracer which had been perfused in to the anterior segment with fluorescent tracer which had been passively soaked into the anterior segment tissue overnight. Amine- and carboxy-modified fluorescent microspheres were either sequentially perfused into anterior segment organ culture as a control, or the green amine-modified microspheres were passively soaked into the tissues overnight, followed by active perfusion of red amine-modified microspheres. After paraformaldehyde fixation, tissues were cut and frontal images were acquired by confocal microscopy. When both
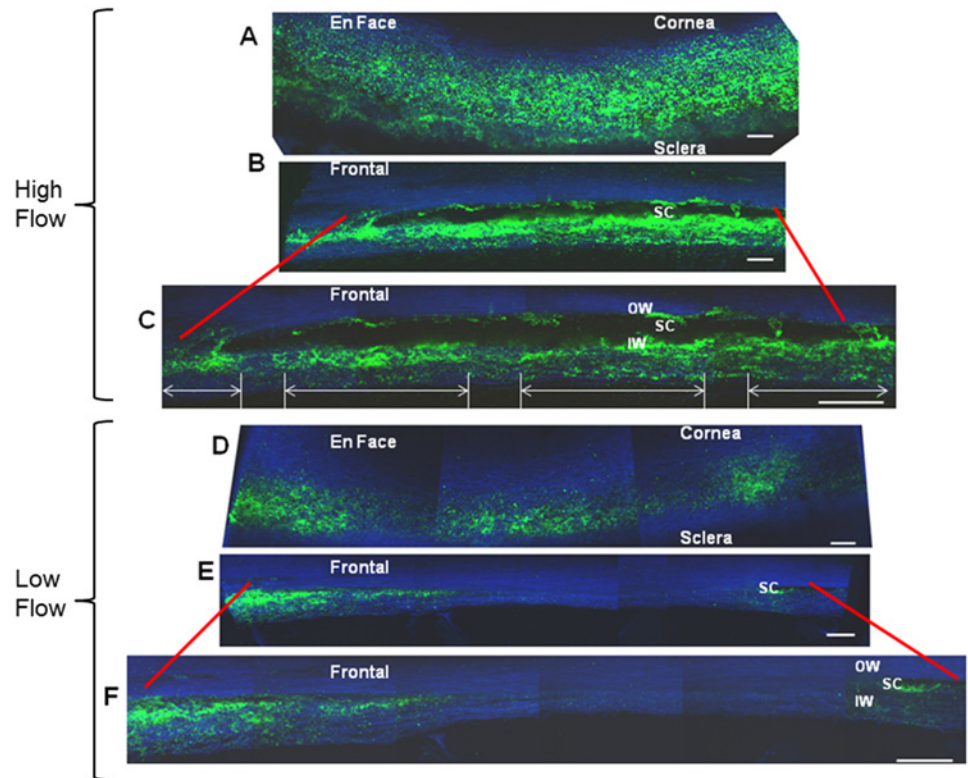
Fig 2. Mapping the flow regions in high and low flow areas of the TM. Human TM sections from high flow (A-C), and medium—low (D-F) flow regions labeled with 200 nm fluorescent amine-modified microspheres (green) are shown *en face* (A and D) or as frontal sections (B, C, E, F). Confocal images of frontal sections show labeling at increasing levels of magnification. High flow regions are shown to contain micro sub-regions of high and low flow (arrows) when viewed at higher magnification (C). Blue color is due to autofluorescence of the TM. Scale bars = 100 μm. OW = Outer wall, SC = Schlemm's canal, IW = Inner wall.

doi:10.1371/journal.pone.0122483.g002

amine- and carboxy-labeled microspheres were sequentially perfused into the tissue they localized to similar areas of the TM (S2 Fig). However, when green fluorescent microspheres were allowed to passively soak into the tissue prior to perfusion of red fluorescent microspheres (S2 Fig), the soaked tracer localized throughout the TM including the low flow regions and into surrounding tissues, whereas localization of the perfused tracer was limited to the putative high flow regions of the TM. This experiment provides further evidence that the perfusion-labeled regions reflect actual fluid flow regions and that segmental difference are not due to the molecular structural components of the TM.

Mapping the Outflow Regions

Next, we further characterized the high and low flow regions. Human anterior segments were perfused with 200 nm green amine-modified fluorescent microspheres and TM tissue was fixed and imaged by confocal microscopy. Representative areas of high and low labeling are shown both *en face* (Fig 2A and 2D) and in frontal sections (Fig 2B-2C and 2E-2F). The representative frontal sections of high flow (Fig 2A-2C) and low flow (Fig 2D-2F) areas are shown at two different magnifications. The low flow regions contained smaller amounts of fluorescent labeling than high flow regions. These images show that at increasing magnification, the distribution of the fluorescent microspheres in high flow regions consists of smaller sub-regions of alternating high flow regions (arrows) interspersed with smaller relatively-low flow regions.
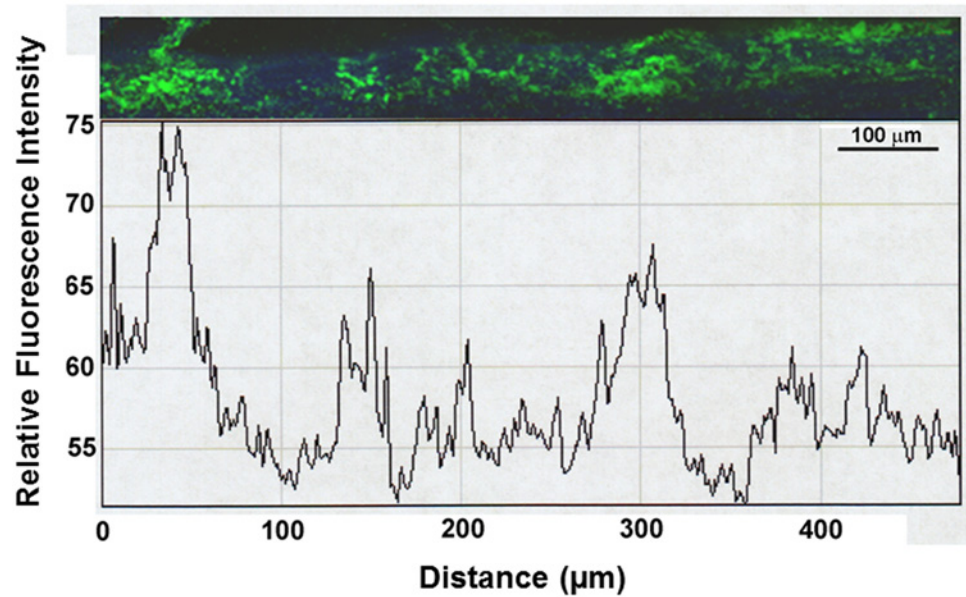
Fig 3. Micro-scale distribution of fluorescent microspheres in a high flow region. High flow regions as shown in Fig 2 were imaged at higher magnification. Relative fluorescent intensity (RFU) was measured across 500 μm and plotted using Image J software. A periodic pattern of micro-flow regions alternating high and low regions (arrows) at approximately every 50–100 μm is shown and originated from a macro high flow TM region. Scale bar = 100 μm.

doi:10.1371/journal.pone.0122483.g003

These high flow sub-regions were approximately 50–100 μm in length (Figs 2C and 3). Relative fluorescence intensity was plotted across 500 μm of a representative high flow region of the TM to graphically demonstrate the periodic distribution of high and low sub-regions contained within a larger high flow region (Fig 3).

Perfusion of Labeled Microspheres Selectively Targets the TM

Versican has been shown previously to selectively label the JCT region of the TM and contains negatively charged glycosaminoglycan side chains which might influence the distribution of amine-modified fluorescent microspheres within the TM. Therefore, fixed tissues that had been perfused with 200 nm amine- and carboxy-modified fluorescent microspheres were immunostained for versican, and high and low flow regions were imaged by confocal microscopy (Fig 4). Distribution of versican immunostain and amine- versus carboxy-labeled microspheres was compared and Imaris software was used to determine Pearson's correlation coefficients. This provides a quantitative assessment of the colocalization between two signals acquired in separate channels. Surprisingly, amine- and carboxy-modified spheres appeared to colocalize moderately with each other, but had very weak colocalization with the versican immunostaining (Fig 4C-4E).

It has previously been shown that collector channels are often found in high flow regions, but low flow regions were not studied in detail.[26,37,47] We wanted to determine the likelihood of finding collector channels in low flow regions of the TM. Thus, after perfusion with amine-modified fluospheres, collector channels were imaged using confocal microscopy. Schlemm's canal was visualized with PECAM immunostain (blue) which specifically localizes to inner wall endothelial cells.[42] Representative images show that collector channels are present both in high flow (Fig 5A) and low flow (Fig 5B) areas of the TM. In both regions, the fluorescent microspheres tended to accumulate in and around Schlemm's canal adjacent to
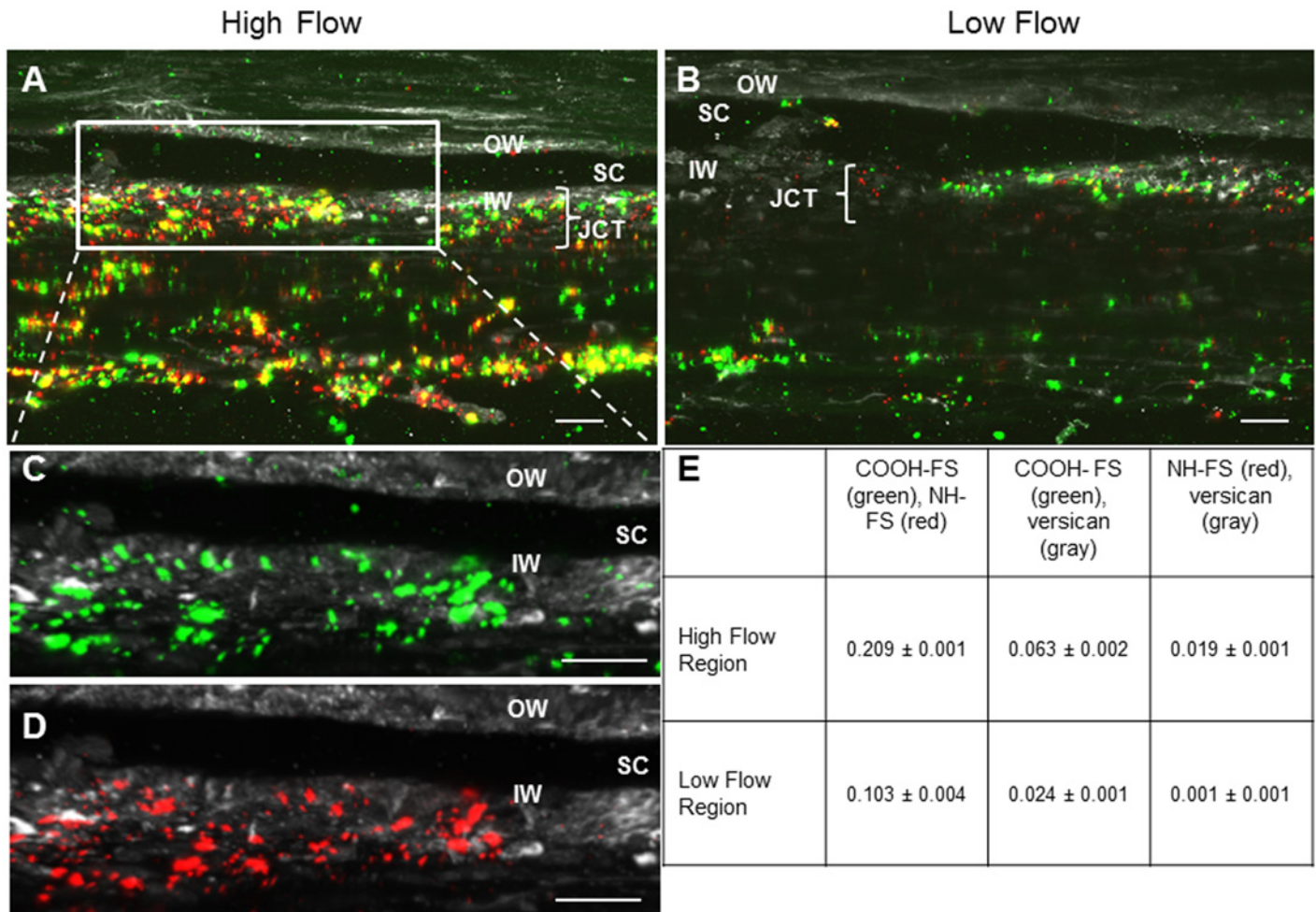
Fig 4. Amine- and carboxy-modified fluorescent microspheres (200 nm) colocalize in high and low flow regions of the TM. Anterior segments were sequentially perfused with 200 nm amine-modified (red) and carboxy-modified (green) fluorescent microspheres prior to fixation and confocal imaging. Confocal images show overlapping red and green in both high (A, C, D) and low (B) flow regions. Immunostaining for versican (gray) localizes to the inner wall and outer wall of Schlemm's canal and to the JCT region of the TM (A-D). Boxed area in A was zoomed and red and green channels were separated to visualize overlap with versican (gray) (C, D). Pearson's correlation coefficients (Pcc) were measured using Imaris software in order to determine the amount of colocalization between two signals €. The amine- and carboxy-modified fluospheres colocalize in both high and low flow regions of the TM; n = 3 for each pairing. Scale bars = 20 μm. OW = Outer wall, SC = Schlemm's canal, IW = Inner wall, JCT = Juxtacanalicular TM.

doi:10.1371/journal.pone.0122483.g004

collector channels when collector channels were present; however no quantitation was done on the relationship between collector channels and bead location.

Gene Expression Differences in High and Low Flow Regions of the TM

ECM is thought to be the source of outflow resistance so we hypothesized that ECM gene expression may be different between regions, which may provide clues as to genes that are important to facilitate aqueous humor outflow. In order to determine molecular differences in ECM genes in high and low flow regions of the TM, RNA was extracted and ECM and adhesion gene quantitative PCR arrays were performed (Fig 6). Fold change values are represented graphically and show gene changes in high flow regions in comparison with low flow regions. The collagen genes COL1A1, COL4A2, COL6A1, COL6A2, and COL16A1, were all more enriched in high flow regions, whereas COL15A1 was enriched in low flow regions. The matrix
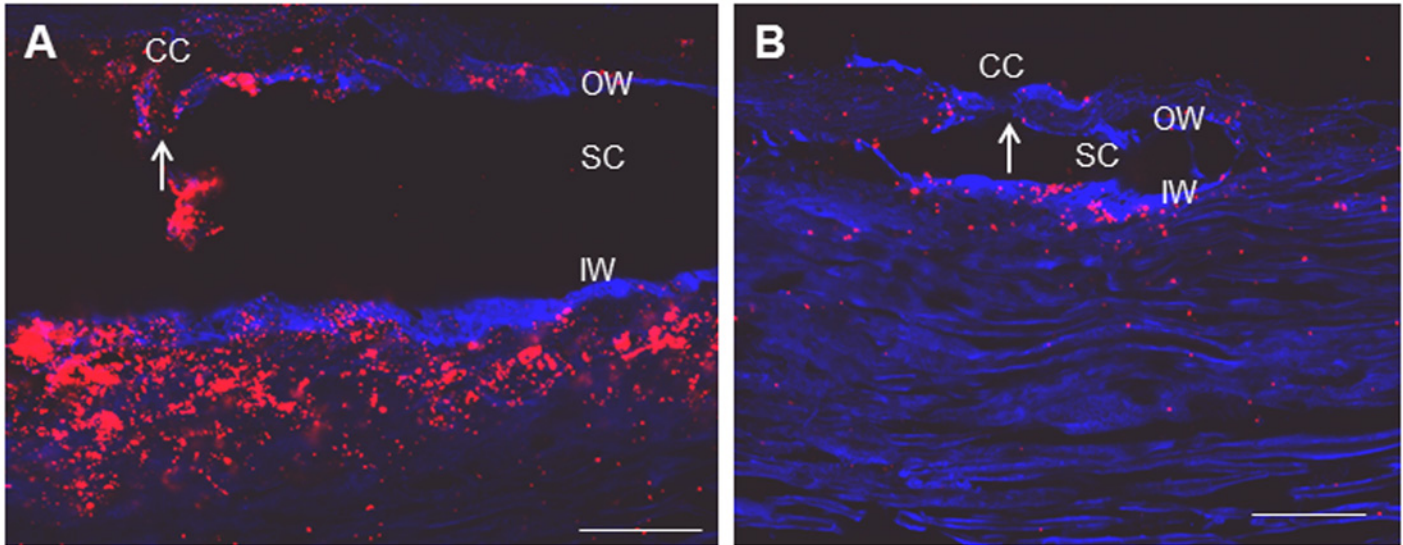
Fig 5. Collector channels are present in high and low flow areas of the TM. Representative images are shown of high (A) and low (B) flow regions of the TM after perfusion with 200 nm amine-modified fluorescent microspheres (red). Fluorescent microspheres appear to accumulate in areas near collector channels (arrows) in both regions. Scale Bar = 50 μm. OW = Outer wall, SC = Schlemm's canal, IW = Inner wall. Blue is PECAM immunostaining to aid in the visualization of Schlemm's canal and collector channels, particularly in low flow regions.

doi:10.1371/journal.pone.0122483.g005

metalloproteinase (MMP) genes MMP1, 2, 3 and 12 were enriched in high flow regions. Conversely, MMP16 was relatively enriched in the low flow regions. Additional differences were seen with the matricellular gene SPARC which was enriched in high flow regions, whereas osteopontin (SPP1) was enriched in low flow regions. Other gene families such as the integrins (ITG) and laminins (LAM) also showed variable expression with some members enriched in high flow regions and others in low flow regions. Thus, there are distinct molecular differences in ECM gene expression levels in high and low flow regions of the TM.

Immunostaining of TM tissues of a select set of proteins, whose genes showed differential expression in high and low flow regions of the TM, was performed to corroborate some of the PCR array data (Fig 7A-7F). Type VI collagen (Fig 7A-7B) and SPARC (Fig 7C-7D) genes were both enriched in high flow regions of the TM and their immunostaining patterns indicate that their proteins are also more enriched in high flow regions, respectively. SPP1, a gene that was slightly more enriched in low flow regions of the TM, only showed minimal differential immunostaining in high (Fig 7E) and low (Fig 7F) flow regions.

MMP Activity Assay

The gene expression data shows enrichment of MMP1, 2 and 3 in high flow regions and, conversely, enrichment of MMP-16 in low flow areas. Immunostaining of high and low flow regions of the TM was performed using an antibody to MMP3 (Fig 8A-8B) and showed increased staining in the high flow regions. Regulation of MMP genes does not necessarily equate to increased activity of the enzymes. To quantitate proteolytic enzyme activity in each outflow region of the tissue, an enzyme assay was performed using a peptide that can be cleaved by multiple MMPs (Fig 8C). There was no significant difference in the total proteolytic MMP enzyme activity in the high flow regions of the tissue compared to the low flow regions. This indicates that although there are individual MMP gene expression differences in the high and low flow regions of the TM, these may not be reflected in overall protein levels or enzyme activities measured on the same regions.
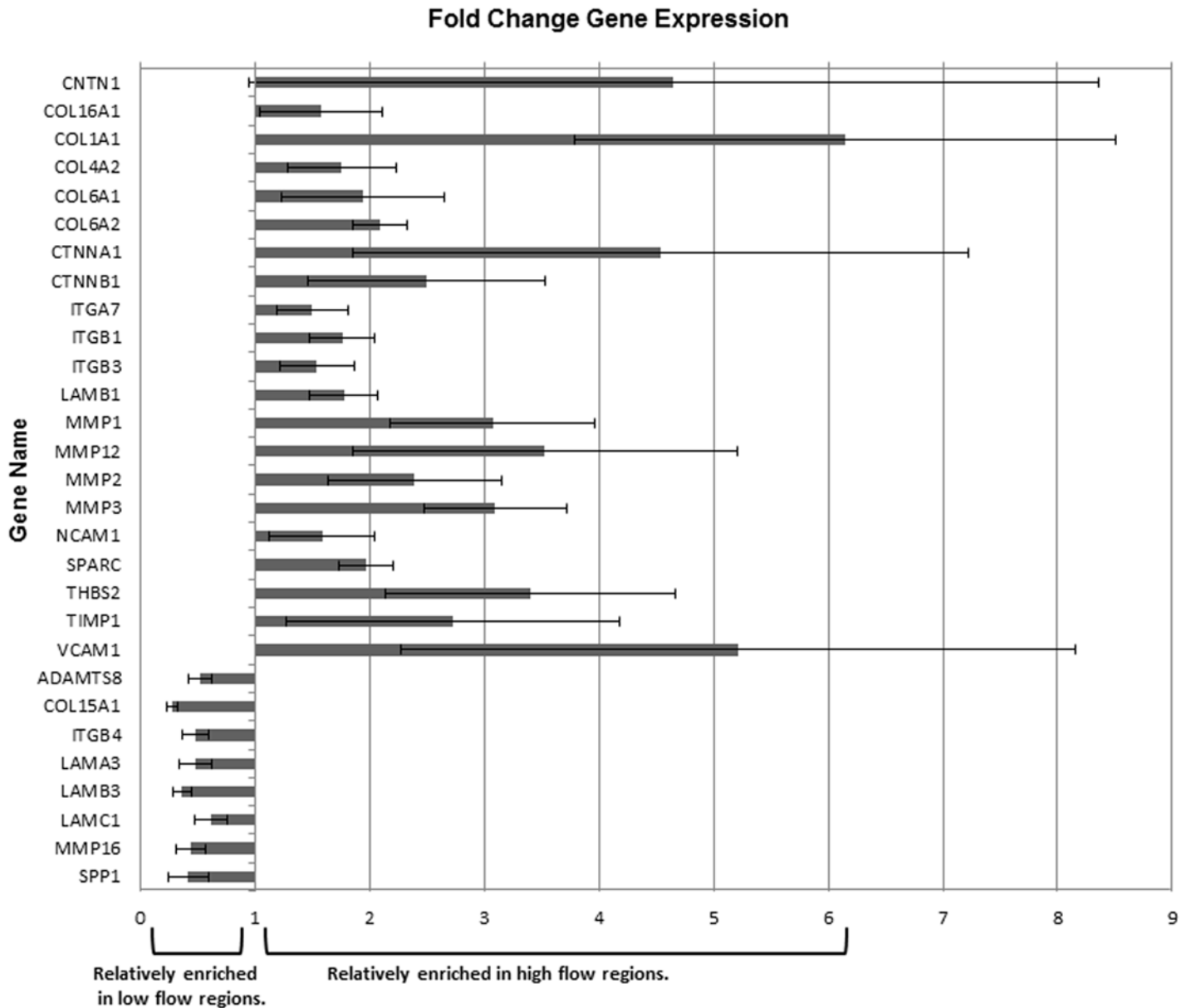
Fig 6. Quantitative PCR array of TM from high flow regions in comparison with low flow regions. Human TM's were dissected from perfused anterior segments, RNA was isolated, reverse transcribed, and measured using the human extracellular matrix and adhesion molecule quantitative PCR array. Fold change gene expression is shown as either enriched in high flow regions (values greater than 1.0) or enriched in low flow regions (values less than 1.0). All fold changes greater than 1.5 fold and less than 0.5 were considered to be biologically significant. SAM (significance analysis of microarrays), version 4.01, with 4 biological replicates, was used to determine statistically significant fold gene expression changes for HF regions in comparison with LF regions. The raw data using the delta delta Ct values for HF and LF regions was normalized, then subjected to SAM analysis. All fold change genes shown here were determined to be statistically significant by SAM, and biologically significant, by our 1.5 and 0.5 fold criteria. Error bars are the s.e.m.; n = 4 high flow and low flow regions from 4 individual donor eyes.

doi:10.1371/journal.pone.0122483.g006

Discussion

In this study, various fluorescent tracers were perfused into human anterior segment organ culture to further define the nature of segmental aqueous humor outflow. Although segmental outflow has been observed for many years, the contributing factors, and its consequences on outflow resistance, remain poorly understood. It is generally believed that regions of high tracer
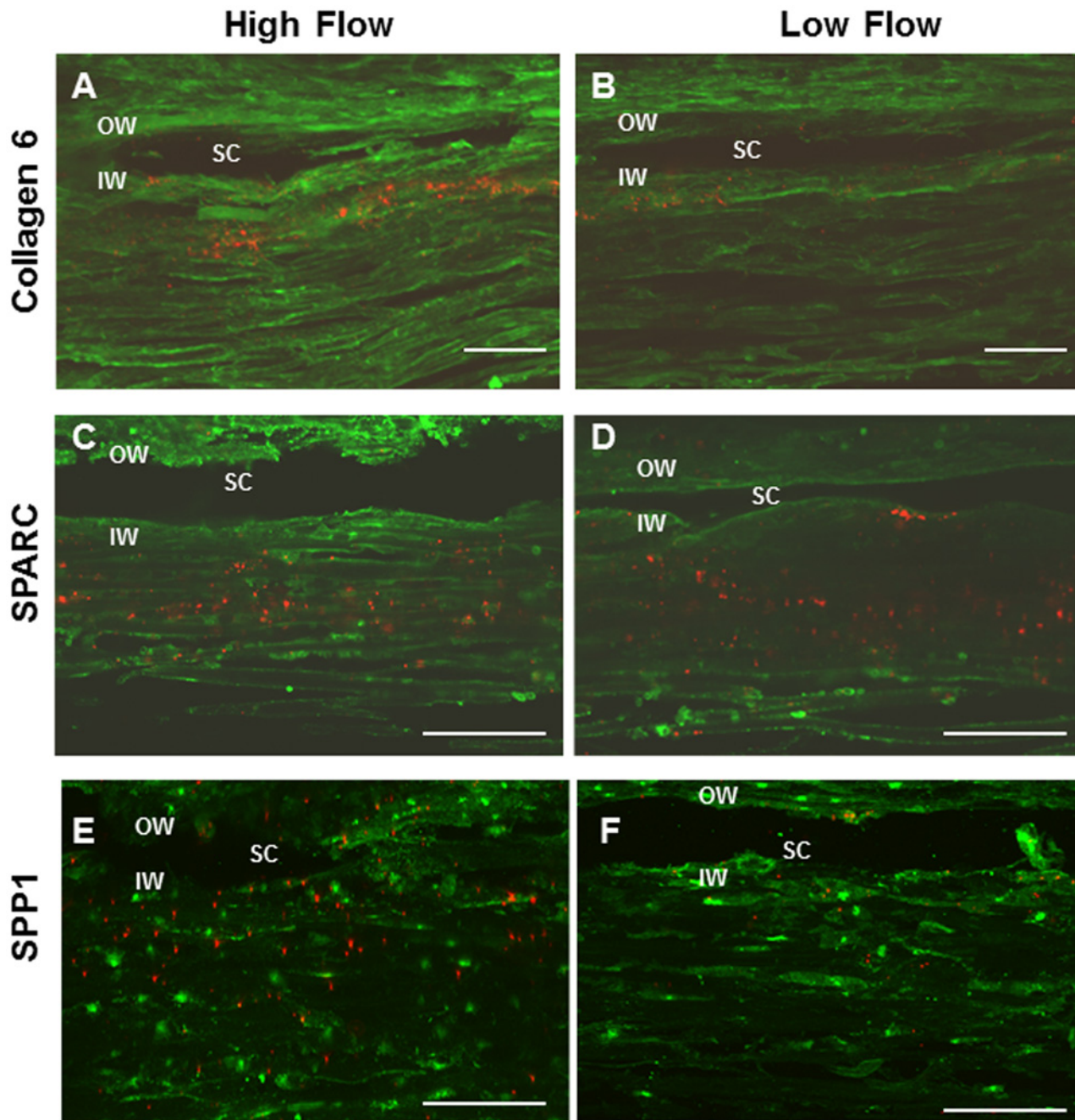
Fig 7. Immunostaining for select ECM proteins in high and low flow regions of the TM. Tissues were perfused with 200 nm amine-modified fluorescent microspheres (red) to separate high (A, C, E) and low (B, D, F) flow regions. Frontal sections were immunostained (green) with antibodies to Type VI collagen (A, B), SPARC (C, D) or SPP1 (E, F) and imaged by confocal microscopy. Scale bar = 50 µm. OW = Outer wall, SC = Schlemm's canal, IW = Inner wall.

doi:10.1371/journal.pone.0122483.g007

labeling are considered areas of high fluid flow across the TM and into Schlemm's canal, whereas regions of low tracer labeling are areas of little to no fluid flow. Our studies using actively perfused microspheres versus passively soaked microspheres supports that tracers are labeling outflow pathways. Our analyses of many perfused human eyes showed some variability in the relative amount of high and low flow regions. However, in general, approximately one-third of the each eye was high flow, one-third low flow, and the remainder was medium
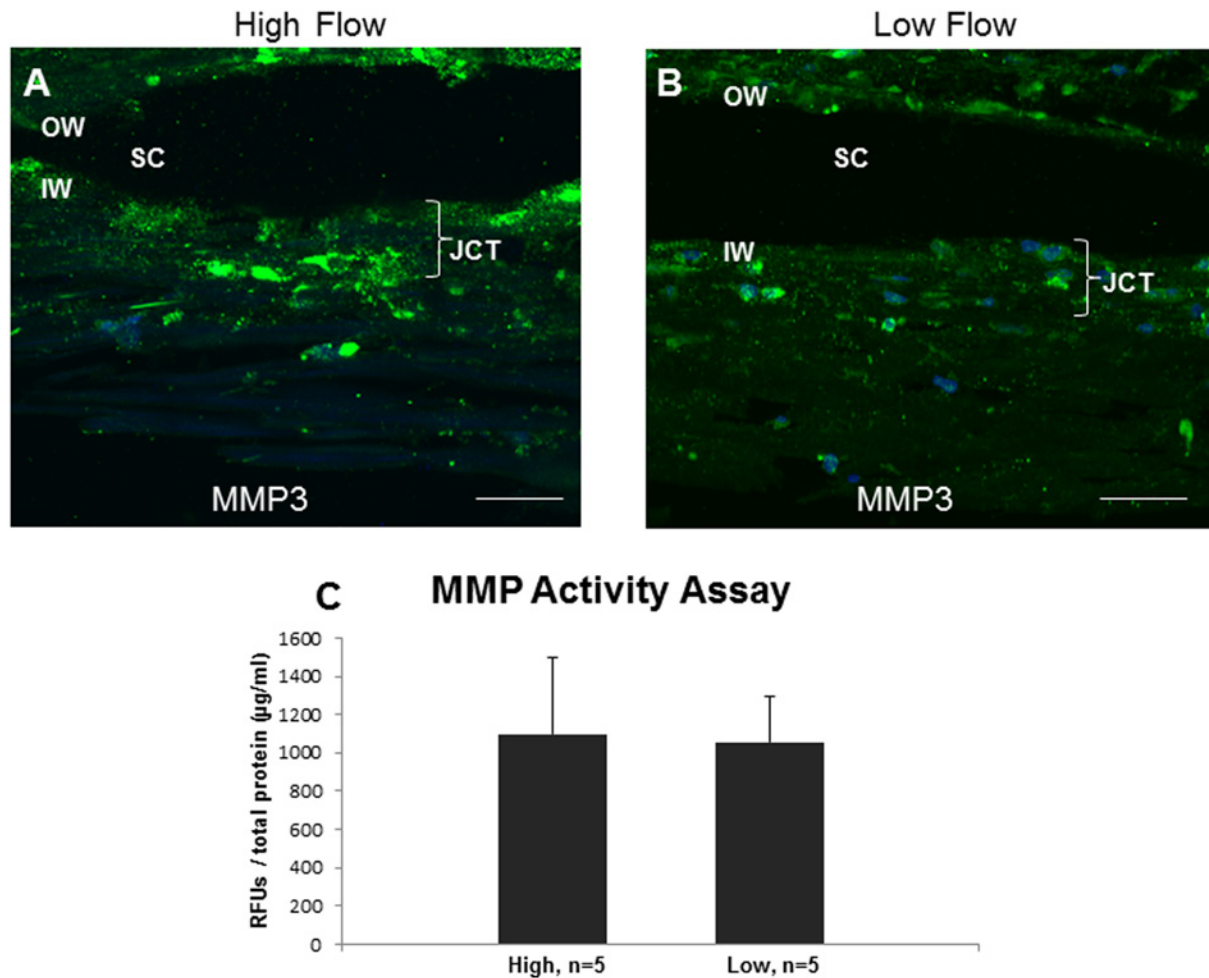
Fig 8. MMP3 immunostaining and MMP activity in high and low flow regions of human TM. Frontal sections of high (A) and low (B) flow regions of human TM from perfused anterior segment organ culture were immunostained with an antibody to MMP3 (green). DAPI is the nuclear stain (blue). Scale bar = 30 μm. OW = Outer wall, SC = Schlemm's canal, IW = Inner wall, JCT = Juxtacanalicular TM. MMP activity in high and low flow regions of human eyes (C). Results are shown as relative fluorescent units (RFUs) normalized to total protein (μg/ml) in each sample. "N" for each region is listed in the graphs.

doi:10.1371/journal.pone.0122483.g008

flow. This is in agreement with a recent study that determined only about one-third of the TM is tracer-labeled and therefore involved in active filtration at any given time.[37]

Initially, we varied the size and the modification of the tracer perfused into the tissue to determine differences in localization patterns throughout the different anatomical layers of the TM. Previous studies have shown that perfused cationic ferritin localizes to different areas of the TM than anionic ferritin and reduces outflow facility.[22] In particular, cationic ferritin was consistently seen on the luminal surface of the inner wall of Schlemm's canal and variably labeled the JCT and trabecular beam surfaces, whereas anionic ferritin was more prominent in the JCT and intertrabecular spaces.[22] It is unclear whether there might be charge-specific interactions with ECM components in the outflow pathway, or whether net charge patterns within the outflow pathway impact flow marker binding, both of which would affect fluid flow across the TM. Fluorescent microspheres with an HIV-TAT modification (20 nm) localized to the outer uveal TM beam region presumably because of highly-active phagocytosis. Similarly-sized microspheres without the HIV-TAT modification did not accumulate in the outer uveal meshwork, but they were more sparsely distributed throughout the layers of the TM. Larger

fluorescent microspheres with amine-modification were more evenly distributed across the TM and, in particular, within the JCT region of the TM

The conventional outflow pathway is an attractive therapeutic target for glaucoma patients since lowering IOP remains the only effective strategy to stop the progression of glaucoma vision loss. However, no drugs are currently in use that target this pathway. In order to target glaucoma drugs to the TM, in-depth knowledge of TM cell biology is required. Gene expression differences between TM beam cells, JCT cells and Schlemm's canal inner wall cells have been reported.[48–50] It is attractive to speculate that by simply varying the size of the tracer, and optimizing the dose and treatment time, different populations of TM cells might be targeted. This feature would be especially beneficial for targeting drug therapies to distinct TM cell populations.

We compared the active perfusion of fluorescent tracer with the passive soaking of fluorescent tracer to determine whether the patterns of segmental outflow are dependent on perfusion. When fluorescent tracer was allowed to soak into the tissues overnight in the absence of perfusion, it was found in all areas of the tissue and no segmental effect was observed. The same tissues were then perfused with a differently-colored fluosphere, and that tracer preferentially localized within the TM and Schlemm's canal. This suggests that although all areas can be labeled equally, segmental outflow requires active perfusion and that only the filtration-active areas are labeled. The biological function of the low flow areas remains unclear at this time. However, even though low flow areas are not involved in filtration, the cells in these regions remain viable as HIV-TAT nanoparticle uptake shows. Interestingly, within areas considered to be high flow, imaging at higher magnification showed micro-scale regions of alternating high and low flow regions of approximately 50–100 μm in length of tracer labeling. This coexistence of macro- and micro-regions of flow areas was also in agreement with recent studies and suggests the possibility that localized ultrastructures within the TM and Schlemm's canal may contribute to the overall outflow resistance around the circumference of the TM.[37,51]

To further address the question of whether charge of the fluorescent tracer may have a preferential fluid flow, due to charge-specific interactions with ECM components in the outflow pathway, tissues were sequentially perfused with amine- and carboxy-modified fluospheres. Then they were immunostained with an antibody to versican and imaged by confocal microscopy. The amount of overlapping signal between the fluospheres and the versican immunostain was quantitated in high and low flow regions. The present study used versican immunostaining to visualize ECM structures within the TM near Schlemm's canal. Since versican is substituted with negatively charged chondroitin sulfate chains, we hypothesized that it would preferentially colocalize with the amine-modified fluorescent microspheres. Pearson's correlation coefficients, which determine the amount of overlapping signal between two channels, were calculated between the carboxy- or the amine-modified fluospheres, and versican immunostaining in the TM. In this study, it was of interest to note that although the carboxy- and amine-modified fluospheres showed a moderate degree of colocalization with each other, both had a very weak association with versican immunostaining. Thus, carboxy- and amine-modified fluorescent microspheres localized to similar areas along the TM suggesting the existence of diverse binding sites within common fluid flow routes of the TM en route to Schlemm's canal and the venous drainage tract.

Studies have confirmed the presence of approximately 25–30 collector channels per eye and determined them to be distributed somewhat unevenly around the circumference of Schlemm's canal.[52–54] Preferential fluid flow has previously been reported to occur near collector channels, particularly in pigmented areas of the TM.[25,47] Recent studies corroborated this finding where high tracer-labeled regions coincided with collector channels. In this study, although we did not rigorously evaluate the relationship of tracer labeling with the presence of collector channels, we observed that the fluorescent tracer often accumulated in the JCT in regions near

collector channels in both high and low flow regions. These observations are in general agreement with several previous studies showing a modest positive correlation of flow and the presence of collector channels.[25,37,47] However, based on our observations, collector channels and flow regions are not strictly correlated. In other words, if a map of collector channels were to be superimposed on the segmental flow regions of an individual eye, it is likely that there would be an equal chance of finding collector channels in the high flow as in the low flow regions. Thus, the relationship of the presence of collector channels and preferential fluid flow may be more complex than previously thought. Carefully-designed statistical regional analyses will be necessary to further clarify the relationship between collector channels and segmental outflow patterns.

Some studies have identified expression differences in ECM components in glaucomatous TM versus normal TM, such as cochlin,[55], matrix gla protein and type V collagen[56], and MMP-1, -10 and microfibril-associated glycoprotein-2[57]; however, these expression differences have not been correlated to segmental flow, except for cochlin which was found in deposits in a segmental manner. Additionally, glaucomatous TM tissue was shown to be stiffer than normal TM tissue, as measured by atomic force microscopy[58], and this difference is thought to be due to differences in ECM components. Studies are currently underway to determine whether there are stiffness differences in the segmental regions of the TM. Apart from versican and SPARC, little is known about the molecular structure and ECM components as they relate to segmental outflow.[17,29] The ECM proteins fibronectin and hyaluronan binding protein were found to have variable patterns of immunostaining, but were not correlated with tracers. [11,40] In order to better understand the ECM involvement in segmental flow, PCR arrays were used to determine ECM gene expression level differences. Several collagen genes, namely COL1A1, COL4A2, COL6A1, COL6A2, and COL16A1, were more than 1.5-fold higher in expression in high flow regions compared with low flow regions. Conversely, COL15A1 was enriched in low flow regions. Mutations in collagen genes have been associated with glaucoma (recently reviewed).[59] Of particular relevance to this study is the observation that genetic variations in COL15A1 can modify the age of onset of early and late onset primary open angle glaucoma.[60–62] Type XV collagen is a fibril-associated collagen that is a component of the basement membrane and may be involved in outflow resistance. Other ECM components such as CTNNB1, MMP2, and MMP3 genes were also more than two-fold higher in expression in high flow regions than in low flow regions. In contrast, the laminins, LAMA3, LAMB3, and LAMC1, as well as MMP16 were all enriched in low flow regions compared with high flow regions. Many previous studies have identified key ECM genes expressed in TM cells and tissues. [2,9,10,63–66] However, this study sheds new light on ECM gene-specific differences in high and low flow regions of the TM.[2,10,20,64]

High flow regions of the tissue appear to show no significant difference in total MMP proteolytic activity than low flow regions; however, the substrate used was a generic MMP substrate. Increases in activity of one MMP may be tempered by decreases in activity of another MMP. More MMP assays using specific MMP substrates may detect differences in individual MMP activities in each segmental outflow region. Previously, we had shown that, unlike many other adult tissues, the TM has high levels of MMP expression.[66–68] We recently proposed that this high MMP expression may be essential for maintenance remodeling of the outflow channels to aid passage of aqueous humor to Schlemm's canal.[3] For instance, debris from aqueous humor may become trapped on the sticky ECM within the outflow channels as fluid passes through the tissue. MMPs may be used to cleave ECM molecules to release the debris and associated ECM fragments in order to prevent blockage and IOP elevation. The PCR array data presented here support the contention that MMPs are likely involved in outflow resistance. The use of new MMP substrates that target individual MMPs will help to dissect which enzyme activities play a role in specific regions of the tissue.

The general acknowledgement of segmental outflow should have significant future impacts on the design and delivery of treatments for glaucoma since high flow regions are inherently over-treated, while low flow areas are under-treated by current drug delivery techniques.. Thus, it will be of importance to determine molecular differences in high and low flow regions that can then be manipulated or targeted individually in future treatments of glaucoma.

Supporting Information

S1 Fig. Segmental flow is independent of tracer size and modification. Confocal images of frontal sections from perfused human anterior segments show representative high (A, C) and low (B, D) flow areas of the TM. In high flow region, Qtracker-655 (20 nm with HIV-TAT modification) (A) is selectively taken up by the outer uveal/corneoscleral TM and thus little labeling is seen in the JCT. In contrast, the 200 nm amine-modified fluorescent microspheres were evenly localized throughout the TM (C). Immunostaining for fibrillin-1 is shown in green and primarily labels the JCT region in all panels. DAPI staining is blue in all panels. Scale Bar = 50 μm. OW = Outer wall, IW = Inner wall, SC = Schlemm's canal, JCT = Juxtacanalicular TM.
(TIF)

S2 Fig. Perfusion of labeled fluorescent microspheres selectively targets the TM. Anterior segments were either sequentially perfused with 200 nm amine-modified (red) and carboxy-modified (green) fluospheres (A–C) or passively soaked with 200 nm amine-modified fluospheres for 20 hours followed by perfusion of 200nm amine-modified fluospheres (green) (D–F). Red and green channels were merged (C and F) and blue color is autofluorescence of TM. Scale Bar = 100 μm. OW = Outer wall, SC = Schlemm's canal, IW = Inner wall.
(TIF)

S1 Table. Donor eye information for all tissues used in study. All relevant biological information regarding the donor and known ocular history is listed.
(DOCX)

Acknowledgments

Author Contributions

Conceived and designed the experiments: JAV KEK TSA. Performed the experiments: JAV JMB YFY. Analyzed the data: JAV KEK TSA. Contributed reagents/materials/analysis tools: JAV JMB YFY KEK TSA. Wrote the paper: JAV.

References

1. Stamer WD, Acott TS (2012) Current understanding of conventional outflow dysfunction in glaucoma. Curr Opin Ophthalmol 23: 135–143. doi: 10.1097/ICU.0b013e32834ff23e PMID: 22262082

2. Acott TS, Kelley MJ (2008) Extracellular matrix in the trabecular meshwork. Exp Eye Res 86: 543–561. doi: 10.1016/j.exer.2008.01.013 PMID: 18313051

3. Keller KE, Acott TS (2013) The Juxtacanalicular Region of Ocular Trabecular Meshwork: A Tissue with a Unique Extracellular Matrix and Specialized Function. J Ocul Biol 1: 3. PMID: 24364042

4. Tamm ER (2009) The trabecular meshwork outflow pathways: structural and functional aspects. Exp Eye Res 88: 648–655. doi: 10.1016/j.exer.2009.02.007 PMID: 19239914

5. Johnson M (2006) 'What controls aqueous humour outflow resistance?'. Exp Eye Res 82: 545–557. PMID: 16386733

6. Gong H, Ruberti J, Overby D, Johnson M, Freddo TF (2002) A new view of the human trabecular mesh-work using quick-freeze, deep-etch electron microscopy. Exp Eye Res 75: 347–358. PMID: 12384097

7. Ethier CR (2002) The inner wall of Schlemm's canal. Exp Eye Res 74: 161–172. PMID: 11950226

8. Lutjen-Drecoll E (1999) Functional morphology of the trabecular meshwork in primate eyes. Prog Retin Eye Res 18: 91–119. PMID: 9920500

9. Bradley JM, Vranka J, Colvis CM, Conger DM, Alexander JP, Fisk AS, et al. (1998) Effect of matrix metalloproteinases activity on outflow in perfused human organ culture. Invest Ophthalmol Vis Sci 39: 2649–2658. PMID: 9856774

10. Keller KE, Bradley JM, Acott TS (2009) Differential effects of ADAMTS-1, -4, and -5 in the trabecular meshwork. Invest Ophthalmol Vis Sci 50: 5769–5777. doi: 10.1167/iovs.09-3673 PMID: 19553617

11. Keller KE, Bradley JM, Kelley MJ, Acott TS (2008) Effects of modifiers of glycosaminoglycan biosynthesis on outflow facility in perfusion culture. Invest Ophthalmol Vis Sci 49: 2495–2505. doi: 10.1167/iovs.07-0903 PMID: 18515587

12. Spiga MG, Borras T (2010) Development of a gene therapy virus with a glucocorticoid-inducible MMP1 for the treatment of steroid glaucoma. Invest Ophthalmol Vis Sci 51: 3029–3041. doi: 10.1167/iovs.09-4918 PMID: 20089870

13. Barany EH, Scotchbrook S (1954) Influence of testicular hyaluronidase on the resistance to flow through the angle of the anterior chamber. Acta Physiol Scand 30: 240–248. PMID: 13158098

14. Francois J, Rabaey M, Neetens A (1956) Perfusion studies on the outflow of aqueous humor in human eyes. AMA Arch Ophthalmol 55: 193–204. PMID: 13282544

15. Grant WM (1963) Experimental aqueous perfusion in enucleated human eyes. Arch Ophthalmol 69: 783–801. PMID: 13949877

16. Keller KE, Sun YY, Yang YF, Bradley JM, Acott TS (2012) Perturbation of hyaluronan synthesis in the trabecular meshwork and the effects on outflow facility. Invest Ophthalmol Vis Sci 53: 4616–4625. doi: 10.1167/iovs.12-9500 PMID: 22695958

17. Keller KE, Bradley JM, Vranka JA, Acott TS (2011) Segmental versican expression in the trabecular meshwork and involvement in outflow facility. Invest Ophthalmol Vis Sci 52: 5049–5057. doi: 10.1167/iovs.10-6948 PMID: 21596823

18. Zhao X, Russell P (2005) Versican splice variants in human trabecular meshwork and ciliary muscle. Mol Vis 11: 603–608. PMID: 16110303

19. Santas AJ, Bahler C, Peterson JA, Filla MS, Kaufman PL, Tamm ER, et al. (2003) Effect of heparin II domain of fibronectin on aqueous outflow in cultured anterior segments of human eyes. Invest Ophthalmol Vis Sci 44: 4796–4804. PMID: 14578401

20. Keller KE, Aga M, Bradley JM, Kelley MJ, Acott TS (2009) Extracellular matrix turnover and outflow resistance. Exp Eye Res 88: 676–682. doi: 10.1016/j.exer.2008.11.023 PMID: 19087875

21. Buller C, Johnson D (1994) Segmental variability of the trabecular meshwork in normal and glaucomatous eyes. Invest Ophthalmol Vis Sci 35: 3841–3851. PMID: 7928181

22. Ethier CR, Chan DW (2001) Cationic ferritin changes outflow facility in human eyes whereas anionic ferritin does not. Invest Ophthalmol Vis Sci 42: 1795–1802. PMID: 11431444

23. Gottanka J, Johnson DH, Martus P, Lutjen-Drecoll E (2001) Beta-adrenergic blocker therapy and the trabecular meshwork. Graefes Arch Clin Exp Ophthalmol 239: 138–144. PMID: 11372544

24. Hann CR, Bahler CK, Johnson DH (2005) Cationic ferritin and segmental flow through the trabecular meshwork. Invest Ophthalmol Vis Sci 46: 1–7. PMID: 15623746

25. Parc CE, Johnson DH, Brilakis HS (2000) Giant vacuoles are found preferentially near collector channels. Invest Ophthalmol Vis Sci 41: 2984–2990. PMID: 10967055

26. Battista SA, Lu Z, Hofmann S, Freddo T, Overby DR, Gong H (2008) Reduction of the available area for aqueous humor outflow and increase in meshwork herniations into collector channels following acute IOP elevation in bovine eyes. Invest Ophthalmol Vis Sci 49: 5346–5352. doi: 10.1167/iovs.08-1707 PMID: 18515571

27. Lu Z, Overby DR, Scott PA, Freddo TF, Gong H (2008) The mechanism of increasing outflow facility by rho-kinase inhibition with Y-27632 in bovine eyes. Exp Eye Res 86: 271–281. PMID: 18155193

28. Lu Z, Zhang Y, Freddo TF, Gong H (2011) Similar hydrodynamic and morphological changes in the aqueous humor outflow pathway after washout and Y27632 treatment in monkey eyes. Exp Eye Res 93: 397–404. doi: 10.1016/j.exer.2011.05.012 PMID: 21669200

29. Swaminathan SS, Oh DJ, Kang MH, Ren R, Jin R, Gong H, et al. (2013) Secreted protein acidic and rich in cysteine (SPARC)-null mice exhibit more uniform outflow. Invest Ophthalmol Vis Sci 54: 2035–2047. doi: 10.1167/iovs.12-10950 PMID: 23422826

30. Zhu JY, Ye W, Gong HY (2010) Development of a novel two color tracer perfusion technique for the hydrodynamic study of aqueous outflow in bovine eyes. Chin Med J (Engl) 123: 599–605. PMID: 20367989

31. Zhu JY, Ye W, Wang T, Gong HY (2013) Reversible changes in aqueous outflow facility, hydrodynamics, and morphology following acute intraocular pressure variation in bovine eyes. Chin Med J (Engl) 126: 1451–1457. PMID: 23595376

32. Johnson DH (1989) Does pigmentation affect the trabecular meshwork? Arch Ophthalmol 107: 250–254. PMID: 2916978

33. Danon D, Goldstein L, Marikovsky Y, Skutelsky E (1972) Use of cationized ferritin as a label of negative charges on cell surfaces. J Ultrastruct Res 38: 500–510. PMID: 4111070

34. de Kater AW, Melamed S, Epstein DL (1989) Patterns of aqueous humor outflow in glaucomatous and nonglaucomatous human eyes. A tracer study using cationized ferritin. Arch Ophthalmol 107: 572–576. PMID: 2705927

35. Epstein DL, Rohen JW (1991) Morphology of the trabecular meshwork and inner-wall endothelium after cationized ferritin perfusion in the monkey eye. Invest Ophthalmol Vis Sci 32: 160–171. PMID: 1987099

36. Melamed S, Freddo TF, Epstein DL (1986) Use of cationized ferritin to trace aqueous humor outflow in the monkey eye. Exp Eye Res 43: 273–278. PMID: 3758226

37. Chang JY, Folz SJ, Laryea SN, Overby DR (2014) Multi-Scale Analysis of Segmental Outflow Patterns in Human Trabecular Meshwork with Changing Intraocular Pressure. J Ocul Pharmacol Ther.

38. Challa P, Luna C, Liton PB, Chamblin B, Wakefield J, Ramabhadran R, et al. (2005) Lentiviral mediated gene delivery to the anterior chamber of rodent eyes. Mol Vis 11: 425–430. PMID: 15988411

39. Oh DJ, Kang MH, Ooi YH, Choi KR, Sage EH, Rhee DJ (2013) Overexpression of SPARC in human trabecular meshwork increases intraocular pressure and alters extracellular matrix. Invest Ophthalmol Vis Sci 54: 3309–3319. doi: 10.1167/iovs.12-11362 PMID: 23599341

40. Floyd BB, Cleveland PH, Worthen DM (1985) Fibronectin in human trabecular drainage channels. Invest Ophthalmol Vis Sci 26: 797–804. PMID: 3891665

41. Erickson-Lamy K, Rohen JW, Grant WM (1991) Outflow facility studies in the perfused human ocular anterior segment. Exp Eye Res 52: 723–731. PMID: 1855546

42. Heimark RL, Kaochar S, Stamer WD (2002) Human Schlemm's canal cells express the endothelial adherens proteins, VE-cadherin and PECAM-1. Curr Eye Res 25: 299–308. PMID: 12658549

43. Keller KE, Yang YF, Sun YY, Sykes R, Acott TS, Wirtz MK (2013) Ankyrin repeat and suppressor of cytokine signaling box containing protein-10 is associated with ubiquitin-mediated degradation pathways in trabecular meshwork cells. Mol Vis 19: 1639–1655. PMID: 23901248

44. Zinchuk V, Zinchuk O, Okada T (2007) Quantitative colocalization analysis of multicolor confocal immunofluorescence microscopy images: pushing pixels to explore biological phenomena. Acta Histochem Cytochem 40: 101–111. PMID: 17898874

45. Zinchuk V, Wu Y, Grossenbacher-Zinchuk O (2013) Bridging the gap between qualitative and quantitative colocalization results in fluorescence microscopy studies. Sci Rep 3: 1365. doi: 10.1038/srep01365 PMID: 23455567

46. Tusher VG, Tibshirani R, Chu G (2001) Significance analysis of microarrays applied to the ionizing radiation response. Proc Natl Acad Sci U S A 98: 5116–5121. PMID: 11309499

47. Hann CR, Fautsch MP (2009) Preferential fluid flow in the human trabecular meshwork near collector channels. Invest Ophthalmol Vis Sci 50: 1692–1697. doi: 10.1167/iovs.08-2375 PMID: 19060275

48. Fuchshofer R, Welge-Lussen U, Lutjen-Drecoll E, Birke M (2006) Biochemical and morphological analysis of basement membrane component expression in corneoscleral and cribriform human trabecular meshwork cells. Invest Ophthalmol Vis Sci 47: 794–801. PMID: 16505009

49. O'Brien ET, Wang Y, Ying H, Yue BY (2014) Differential expression of genes in cells cultured from juxtacanalicular trabecular meshwork and Schlemm's canal. J Ocul Pharmacol Ther 30: 291–299. doi: 10.1089/jop.2013.0189 PMID: 24611521

50. Perkumas KM, Stamer WD (2012) Protein markers and differentiation in culture for Schlemm's canal endothelial cells. Exp Eye Res 96: 82–87. doi: 10.1016/j.exer.2011.12.017 PMID: 22210126

51. Overby DR, Zhou EH, Vargas-Pinto R, Pedrigi RM, Fuchshofer R, Braakman ST, et al. (2014) Altered mechanobiology of Schlemm's canal endothelial cells in glaucoma. Proc Natl Acad Sci U S A.

52. Dvorak-Theobald G (1955) Further studies on the canal of Schlemm; its anastomoses and anatomic relations. Am J Ophthalmol 39: 65–89. PMID: 14361607

53. Hann CR, Bentley MD, Vercnocke A, Ritman EL, Fautsch MP (2011) Imaging the aqueous humor outflow pathway in human eyes by three-dimensional micro-computed tomography (3D micro-CT). Exp Eye Res 92: 104–111. doi: 10.1016/j.exer.2010.12.010 PMID: 21187085

54. Rohen JW, Rentsch FJ (1968) [Morphology of Schlemm's canal and related vessels in the human eye]. Albrecht Von Graefes Arch Klin Exp Ophthalmol 176: 309–329. PMID: 5305008

55. Bhattacharya SK, Rockwood EJ, Smith SD, Bonilha VL, Crabb JS, Kuchtey RW, et al. (2005) Proteomics reveal Cochlin deposits associated with glaucomatous trabecular meshwork. J Biol Chem 280: 6080–6084. PMID: 15579465

56. Liu Y, Allingham RR, Qin X, Layfield D, Dellinger AE, Gibson J, et al. (2013) Gene expression profile in human trabecular meshwork from patients with primary open-angle glaucoma. Invest Ophthalmol Vis Sci 54: 6382–6389. doi: 10.1167/iovs.13-12128 PMID: 24003086

57. Liton PB, Luna C, Challa P, Epstein DL, Gonzalez P (2006) Genome-wide expression profile of human trabecular meshwork cultured cells, nonglaucomatous and primary open angle glaucoma tissue. Mol Vis 12: 774–790. PMID: 16862071

58. Last JA, Pan T, Ding Y, Reilly CM, Keller K, Acott TS, et al. (2011) Elastic modulus determination of normal and glaucomatous human trabecular meshwork. Invest Ophthalmol Vis Sci 52: 2147–2152. doi: 10.1167/iovs.10-6342 PMID: 21220561

59. Vranka JA, Kelley MJ, Acott TS, Keller KE (2014) Extracellular matrix in the trabecular meshwork: Intraocular pressure regulation and dysregulation in glaucoma. Experimental Eye Research In press.

60. Wiggs JL, Hauser MA, Abdrabou W, Allingham RR, Budenz DL, Delbono E, et al. (2013) The NEIGHBOR consortium primary open-angle glaucoma genome-wide association study: rationale, study design, and clinical variables. J Glaucoma 22: 517–525. doi: 10.1097/IJG.0b013e31824d4fd8 PMID: 22828004

61. Wiggs JL, Howell GR, Linkroum K, Abdrabou W, Hodges E, Braine CE, et al. (2013) Variations in COL15A1 and COL18A1 influence age of onset of primary open angle glaucoma. Clin Genet 84: 167–174. doi: 10.1111/cge.12176 PMID: 23621901

62. Wiggs JL, Pierce EA (2013) Genetic testing for inherited eye disease: who benefits? JAMA Ophthalmol 131: 1265–1266. doi: 10.1001/jamaophthalmol.2013.4509 PMID: 23949187

63. Hann CR, Fautsch MP (2011) The elastin fiber system between and adjacent to collector channels in the human juxtacanalicular tissue. Invest Ophthalmol Vis Sci 52: 45–50. doi: 10.1167/iovs.10-5620 PMID: 20720231

64. Keller KE, Kelley MJ, Acott TS (2007) Extracellular matrix gene alternative splicing by trabecular meshwork cells in response to mechanical stretching. Invest Ophthalmol Vis Sci 48: 1164–1172. PMID: 17325160

65. Keller KE, Vranka JA, Haddadin RI, Kang MH, Oh DJ, Rhee DJ, et al. (2013) The effects of tenascin C knockdown on trabecular meshwork outflow resistance. Invest Ophthalmol Vis Sci 54: 5613–5623. doi: 10.1167/iovs.13-11620 PMID: 23882691

66. Vittal V, Rose A, Gregory KE, Kelley MJ, Acott TS (2005) Changes in gene expression by trabecular meshwork cells in response to mechanical stretching. Invest Ophthalmol Vis Sci 46: 2857–2868. PMID: 16043860

67. Alexander JP, Samples JR, Van Buskirk EM, Acott TS (1991) Expression of matrix metalloproteinases and inhibitor by human trabecular meshwork. Invest Ophthalmol Vis Sci 32: 172–180. PMID: 1846130

68. Bradley JM, Kelley MJ, Zhu X, Anderssohn AM, Alexander JP, Acott TS (2001) Effects of mechanical stretching on trabecular matrix metalloproteinases. Invest Ophthalmol Vis Sci 42: 1505–1513. PMID: 11381054